Simulation Study on the Static Characteristics of 'Five-tier Outer Eave Column-head Dougong Bracket' from Yanghe Tower in Yuan Dynasty

Yuanhe Li,[a] Jiaji He,[a] and Lihong Yao [b,]*

Finite element analysis (FEA) was used to investigate the static structural behavior of the 'Five-tier Outer Eave Column-head Dougong bracket' of the Yanghe Tower from the Yuan Dynasty. Based on GB/T standard testing results for the mechanical properties of *Pinus sylvestris*, an improved ANSYS orthotropic anisotropic model was established. The Hill yield criterion was applied to characterise the wood's plasticity. The model was calibrated against experimental results in the literature. Through simulations of vertical monotonic loading (Z-axis) and horizontal low-cycle cyclic loading (Y-axis and X-axis), the structure's strength, deformation, and energy dissipation capacity were analysed. Results indicate that the maximum vertical bearing capacity at the interface between the *Huagong*-rear-end/*Sandou* interface reached 343 kN, with peak stress reaching 16.9 MPa. Horizontal loading produced symmetric hysteretic curves, with maximum horizontal thrusts of 737 kN (Y-axis) and 523 kN (X-axis). The ductility coefficients were 2.59 and 3.59 respectively, while equivalent viscous damping coefficients were 0.072 and 0.144. Vertical response conformed to a trilinear stiffness degradation model, whilst horizontal response followed a multilinear restoring force model. It was found that finite element analysis (FEA) provided an economical and reliable method for evaluating the mechanical performance of Dougong, offering significant reference value for the conservation of timber heritage structures.

DOI: 10.15376/biores.21.2.3284-3299

Keywords: Dougong bracket; Yanghe Tower; Static characteristics; Finite element simulation; Pinus sylvestris

*Contact information: a: School of Architecture and Art Design, Inner Mongolia University of Science & Technology, Baotou 014010, P.R. China; b: School of Material Science and Art Design, Inner Mongolia Agricultural University, Hohhot 010018, P.R. China; *Corresponding author: yaolihong@imau.edu.cn*

INTRODUCTION

Yanghe Tower (Fig. 1) is situated in Zhengding County, Hebei Province, China. Constructed in 1250 AD during the early Yuan Dynasty, it was demolished in the 1960s and subsequently reconstructed. Sicheng Liang, a pioneering architectural historian, acclaimed its significance: 'The Yanghe Tower stands as majestic as the Arch of Constantine in Rome's Constantinople. Its bracket system is quite rare. This structure inherits the architectural legacy of the Song Dynasty while pioneering Ming-style construction techniques, it is an outstanding representative of the architectural structure from the Yuan Dynasty.' As a quintessential component of ancient Chinese timber architecture, the dougong bracket set is positioned between the column shaft and the roof structure. Through its distinctive interlocking bracket assembly, it both extends the deep

eaves and reduces the span of the beams, while effectively transferring the weighty roof load to the supporting columns (Fang *et al.* 2001; D'Ayala *et al.* 2008; Cao *et al.* 2022). The bucket arch disperses the force of the eaves by jumping outward and transmits it downward, and the bucket arch of the Yanghe Building column head jumps outward twice, and according to the naming of the Chinese bucket arch, the bucket arch is a five-level bucket arch, and the number of stages of the bucket arch should add three to the number of jumps. The cantilever beam extended by the two jumps of the bucket arch is called Ang, and the function of Ang is to effectively extend outward without causing the eaves to rise excessively. The lower layer appears as a horizontal component, called false ang, and the upper layer is true ang (Fig. 2). In the construction of this bucket arch, multi-layer beams are used to form a more complex and stable structure. Multi-layer beams are often used to carry large loads, in this way enhancing the stability and aesthetics of buildings. The practice of the bucket arch of the pillar head of Yanghe Building enhances the bearing capacity of the bucket arch and makes the building more stable in the face of external loads. This structural form not only focuses on practicality, but also emphasizes the aesthetics of the building.

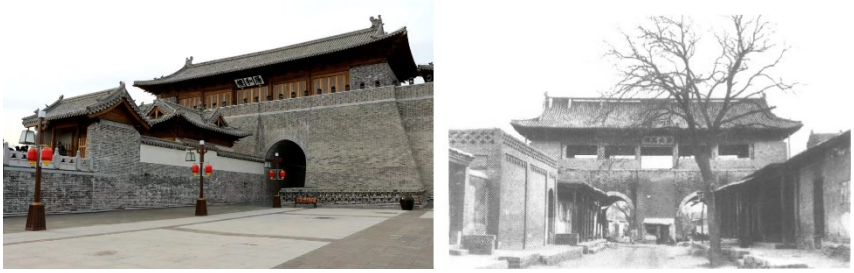

Fig. 1. Yanghe Tower

Fig. 2. Yanghe Tower's column cap and bracket

Following the modular system prescribed in *Yingzao Fashi* (Rules of Architecture, Song Dynasty), Dougong brackets are classified into eight grades based on dimensional hierarchies, each with distinct scale factors tailored to buildings of varying magnitudes (Christovasilis *et al.* 2009; Song *et al.* 2019; Zhang *et al.* 2024). In accordance with *Yingzao Fashi* (Song Dynasty architectural treatise), the dougong bracket examined in this study corresponds to the third-grade timber within the cai-fen modular system (Chen *et al.* 2025). As stipulated in the treatise, one fen° unit for the third-grade timber is defined as 15.5 mm. Specifically, the research examines the Dougong located above the column of Yanghe

tower, comprising 54 modular units—36 primary members and 18 wooden pins—categorized into load-bearing and connective types. Figures 3 and 4 illustrate the test model's perspective view and exploded assembly, delineating its hierarchical composition.

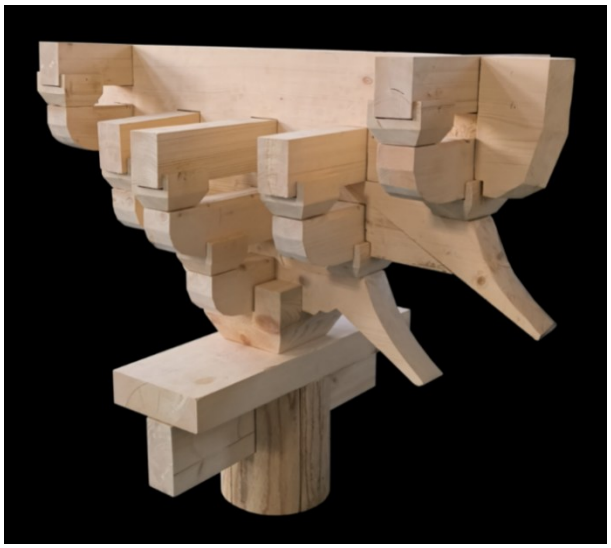

Fig. 3. Perspective view of the Yuan Dynasty bracket structure experimental model

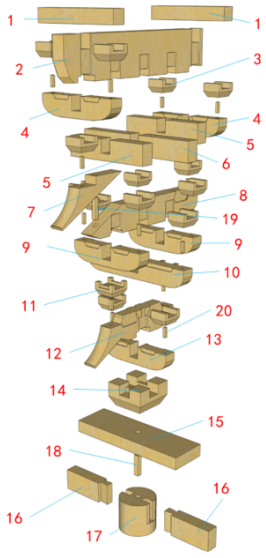

1-Liaoyanfang (Eaves-bearing Structural Beam)
2-Rufu (Vertical beam on the column)
3-San Dou (Dispersed Block)
4-Linggong (Outer Bracket Arm)
5-Zhutoufang (Bear load transfer)
6-Luohanfang (Enhance stability)
7- Ang (Blossoming Bracket Arm)
8-Liangfu (Longitudinal Beam)
9-Guazigong (Short Arm Bracket)
10-Mangong (Horizontal Purlin)
11-Jiaohu Dou (Mutual-Support Block)
12-Huagong (Blossoming Bracket Arm)
13-Nidaogong (Central-axis Bracket Arm)
14-Ludou (Base Bracket Block)
15-Pingbanfang (Dougong Base)
15-Efang (Column Connection Component)
17-Zhutou (Column-top Load-bearing Hub)
18-Wooden Tenon Pin 1
19-Wooden Tenon Pin 2
20-Wooden Tenon Pin 3

Fig. 4. The exploded assembly diagram of 'Column-head Dougong Bracket' test model of the Yanghe Tower

The experimental investigation of traditional timber structures faces significant economic challenges, particularly in constructing full-scale Dougong bracket models, which require substantial material and labor investments (Meng *et al.* 2018; Xian *et al.* 2025). Conventional mechanical testing methodologies, dependent on points measured by instruments, are inherently limited by systematic deviation and spatial resolution constraints, compromising data reliability in complex structural systems (Deng *et al.* 2023;

Meng *et al.* 2019). In contrast, finite element analysis (FEA) has emerged as a robust computational tool for characterizing Dougong mechanics, validated through three decades of methodological refinement and empirical verification (Christovasilis *et al.* 2009; Bedon *et al.* 2015; Zhang *et al.* 2023). This paradigm shift offers dual advantages: 1) elimination of physical specimen fabrication costs, and 2) precise control over boundary conditions and material anisotropy, enabling targeted analysis of critical structural interfaces (Ou and Wang 2023; Sha *et al.* 2021; Wu *et al.* 2022).

This study employs an advanced high-fidelity finite element analysis framework to investigate the static performance of a five-tiered Dougong bracket system supporting the eaves columns. The computational model incorporates three fundamental mechanical indices: (1) Strength characteristics: Ultimate bearing capacity and stress distribution patterns; (2) Deformation mechanisms: Stiffness degradation and displacement gradients; and (3) Energy dissipation: Hysteretic energy absorption and equivalent viscous damping. Through systematic simulation of vertical (Z-axis) monotonic and horizontal (X/Y-axis) low-cycle loading protocols, this research establishes a validated numerical approach for heritage timber structure assessment. The methodology demonstrates a high level of correlation with physical test data while significantly reducing experimental costs, offering an efficient approach for analyzing historical construction techniques and supporting conservation strategies.

EXPERIMENTAL

Finite Element Simulation

The finite element model used *P. Sylvestris* timber conditioned to 12% moisture content. Mechanical properties were determined through standardized tests: air-dry density measured 0.493 g/cm³ (GB/T 1933-2009), while elastic moduli (E), Poisson's ratios (ν), and shear moduli (G) were quantified *via* strain gauge methods (GB/T 15777 2017, GB/T 1943 2009, LY/T 3297 2022). Strength tests yielded a longitudinal compressive strength of 35.2 MPa (GB/T 1935 2009), transverse compressive strength of 17.1 MPa (GB/T 1939-2009), and flexural strength of 52.9 MPa (GB/T 1936.1 2009), as summarized in Table 1.

Table 1. The Poisson's Ratio, Shear Modulus, and Elastic Modulus of *P. sylvestris*

	E_T	E_R	E_L	V_{LR}	V_{RT}	V_{LT}	G_{LT}	G_{LR}	G_{RT}
P. sylvestris	843	1103	8023	0.422	0.687	0.513	345	652	231

* *E* denotes the elastic modulus, in units of MPa; *G* denotes the shear modulus, in units of MPa; *V* denotes the Poisson's ratio, a dimensionless quantity; *T* denotes the tangential direction; *R* denotes the radial direction, and *L* denotes the longitudinal direction; E_T denotes the horizontal tangential elastic modulus, expressed in megapascals (MPa); E_R denotes the horizontal radial elastic modulus, expressed in megapascals (MPa); E_L denotes the modulus of elasticity in the direction of the wood grain, measured in megapascals (MPa); V_{LR} denotes the Poisson's ratio for tensile stress applied along the grain direction of timber; V_{RT} denotes the Poisson's ratio of the tangential extensional stress in the transverse direction; G_{LT} denotes the shear modulus of the string surface along the wood grain, measured in megapascals (MPa); V_{LT} is the Poisson's ratio of transverse radial extension stress; G_{LR} *denotes the radial shear modulus in the direction of the wood grain, measured in megapascals (MPa)*; G_{RT} denotes the horizontal shear modulus, expressed in megapascals (MPa*). All values correspond to the same moisture content (12%).*

The Dougong bracket finite element model was developed in ANSYS Workbench 2021 R1 using a multi-physics framework. Material parameters were calibrated against experimental data, with plasticity modeled via Hill's anisotropic yield criterion and elasticity via orthotropic constitutive relations (Yao and Li 2023). The timber's orthotropic behavior was defined by nine elastic constants: three Young's moduli (E_L, E_R, E_T), three shear moduli (V_{LR}, V_{LT}, V_{RT}), and three Poisson's ratios (G_{LR}, G_{LT}, G_{RT}).

Loading Protocol

The experimental loading protocol adhered to the coordinate system defined in Fig. 5. For vertical loading, monotonic static forces (Xue *et al.* 2022) were placed along the Z-axis to simulate permanent roof loads. For horizontal loading, bidirectional low-cycle alternating displacements (Chen *et al.* 2018; Kaori 2019) were exerted along the Y- and X-axes to replicate seismic actions.

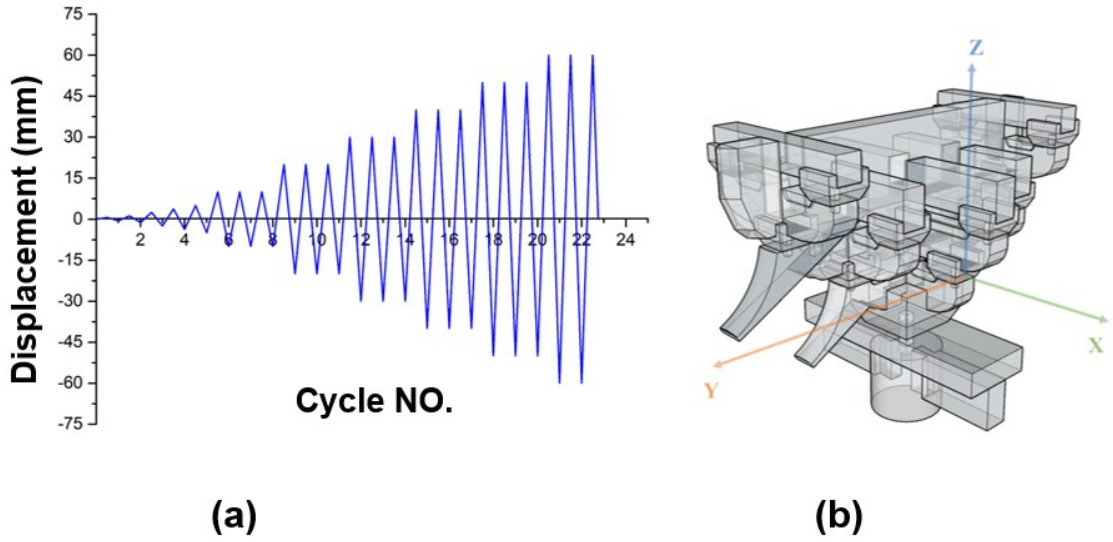

Fig. 5. The loading protocol (a) and specification of the test model's alignment relative to the coordinate axes (b)

Vertically oriented monotonic static tests were performed in accordance with the test method developed by Niu (2017) to simulate the transfer mechanism of permanent roof loads in conventional Chinese Dougong systems. A primary perpendicular load of 60 kN was applied, corresponding to the computed permanent rooftop load based on scale of the building and constructional judgment. A hybrid force-displacement control strategy was employed across two consecutive stages. In the first stage, the test employs a force control scheme at a constant rate of 5 kN/min until the specimen reaches yield, identified through visual morph or pronounced nonlinearity in the load-displacement response. The trial then proceeded to the second phase under displacement control at a rate of 2 mm/min to examine post-succumbing conduct. Ending standard during this stage contained either structural toppling—defined as a reduction in load volume to 80% of the spike resistive—or severe impair that impeded additional loading. This two-phase methodology enabled overall capture of both elastic and plastic strain features while ensuring controlled observation throughout the invalidation process.

Under low-cycle reciprocating loads, quasi-static tests were conducted with displacement control regulation (Yao and Li 2023). The loading mechanism comprises two cycles: The first is a primary cycle, the second comprises five reciprocating cycles with increasing amplitude (0.0125Δ, 0.025Δ, 0.05Δ, 0.075Δ and 0.1Δ, where Δ = 50 mm); Next phase - Commencing at 0.2Δ, each amplitude proficiency level comprises three return cycles, with the incremental amplitude rising by 0.2Δ for each pacing increment (Cao *et al.* 2022). Figure 5 outlines the loading protocol (a) and numerical modelling setup (b). The analytical configuration, connection relevance, and boundary criteria within the model are strictly aligned along the Z, Y, and X axes respectively with the experimental apparatus.

Grid System

A second-order element mesh system was employed, utilizing a hexahedral-tetrahedral hybrid meshing strategy. Regular geometric regions were discretized using hexahedral elements. Within regions of complex geometry, tetrahedral elements are employed. The ultimately assembled mesh system of the Dougong stent is rendered in Fig. 6.

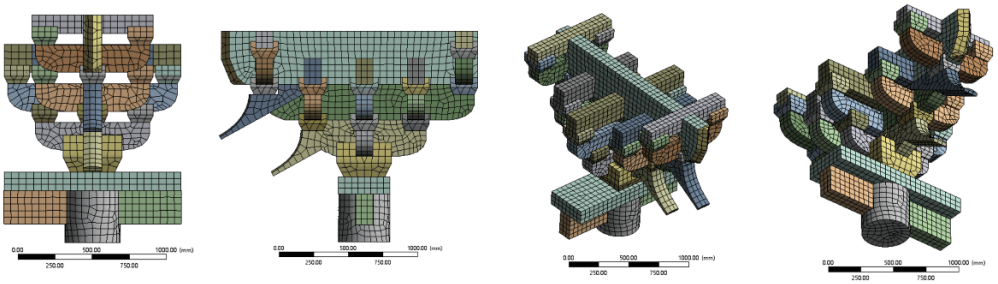

Fig. 6. Classification of Simulated Dougong Bracket Grid Systems

RESULTS AND DISCUSSION

Vertical Monotonic Static Load in the Z-Axis Direction

Figure 7 displays the load-displacement curve obtained by simulating the application of a vertical monotonic load along the Z-axis. The simulated bearing capacity of the bracket model for the Dougong system fails to converge beyond 342.9 kN. Z-axis load analysis (Fig. 8A) indicates that the Von Mises stress in Yuan dynasty Dougong is primarily borne by the upper structural elements along the loading axis. The peak stress magnitude was 16.9 MPa, located at the rear end of the *Huagong structure/ Sandou* interface, corresponding to the central mortise-and-tenon joint. An isometric distribution pattern is observed in the equivalent elastic strain distribution. (Fig. 8B), the maximum strain value at this critical structural interface is 0.039. The strain energy density distribution (Fig. 8C) corresponds to the stress concentration zone, reaching a peak value of 2750 MJ at the *Ludou/Huagong* interface. Such phenomenon of energy concentration demonstrates the effective load transfer mechanism of the dougong system from the upper components to the supporting columns. Displacement analysis of this Dougong (Fig. 8D) reveals that at the apex of the *Liaoyanfang*, the gradient of progressive deformation gradually diminishes from 10.3 mm onwards. This phenomenon aligns with the characteristic progressive deformation of traditional timber structures under vertical loading.

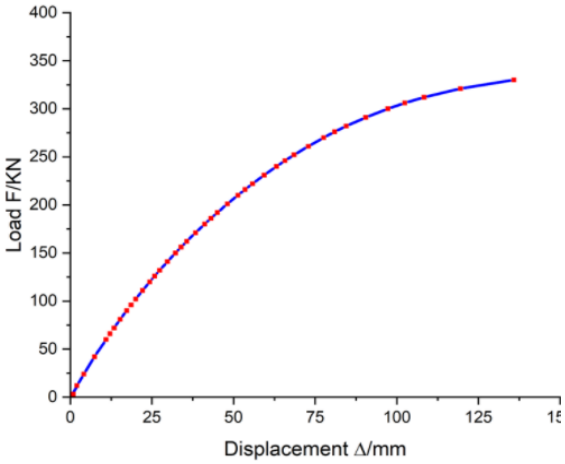

Fig. 7. Z-axis load-displacement curve

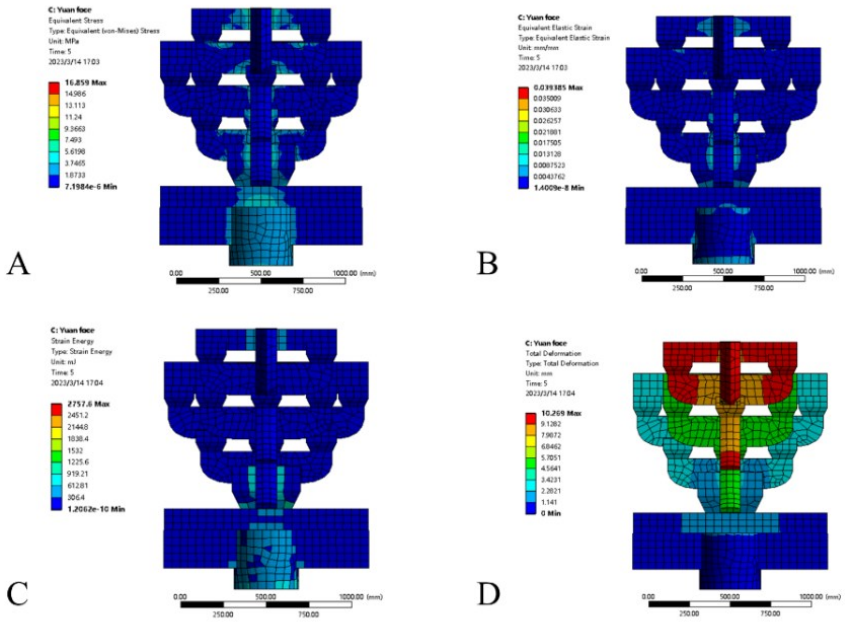

Fig. 8. Von Mises stress distribution along the Z-axis, equivalent elastic strain distribution, energy density distribution of the weighting matrix, and displacement analysis

Low-Cycle Reciprocating Loads on the Y-axis and X-axis

Figure 9 illustrates the load-displacement hysteresis characteristics of the dougong bracket, obtained from simulations of horizontal low-cycle reversed loading tests along the Y and X axes. The peak lateral load capacity of the experimental model in the Y-axis direction and the peak lateral load capacity in the X-axis direction are 737 and 523 kN respectively. Both axial lag curves are spindle-shaped and mutually symmetrical. The observed behavior indicates that the dougong exhibits a significant capacity for plastic deformation under cyclic loading and effectively dissipates energy.

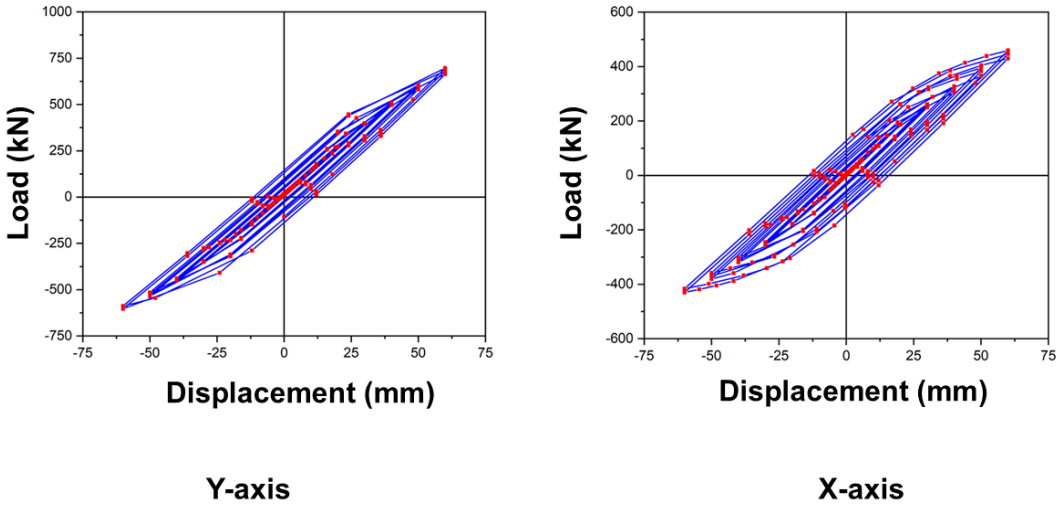

Fig. 9. Y-axis and X-axis load-displacement hysteresis curve diagram

As depicted in the lag curve diagram, the load-displacement skeleton curve diagram can be obtained (Fig. 10), and the rigidity of each segment is extracted from the skeletal curve to derive the specimen's stiffness degradation curve (Fig. 11).

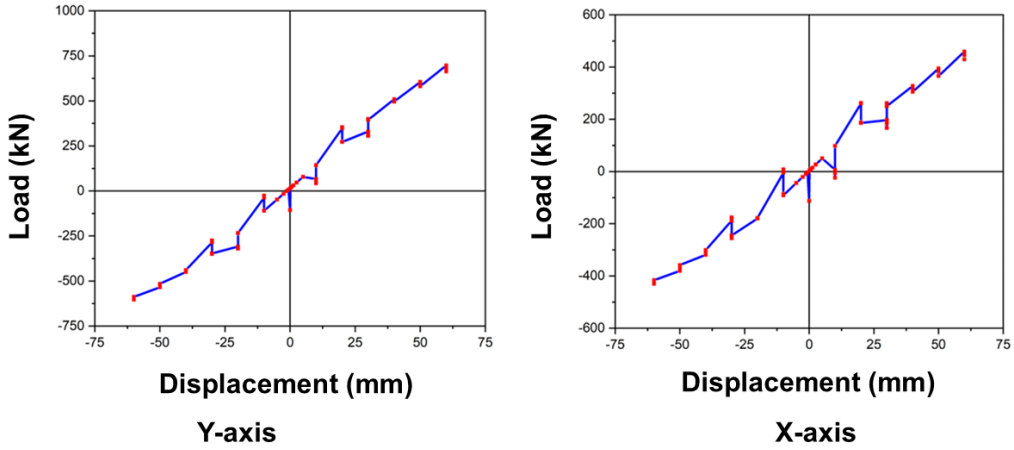

Fig. 10. Y-axis and X-axis load-displacement skeleton curve diagram

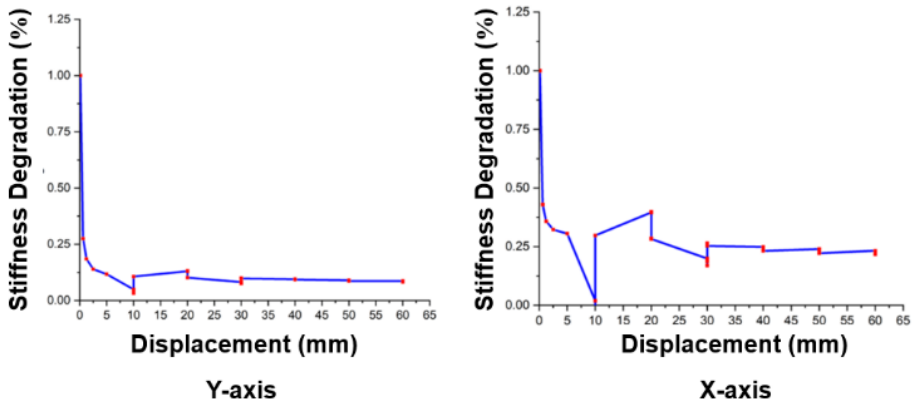

Fig. 11. Y-axis and X-axis stiffness decay curves

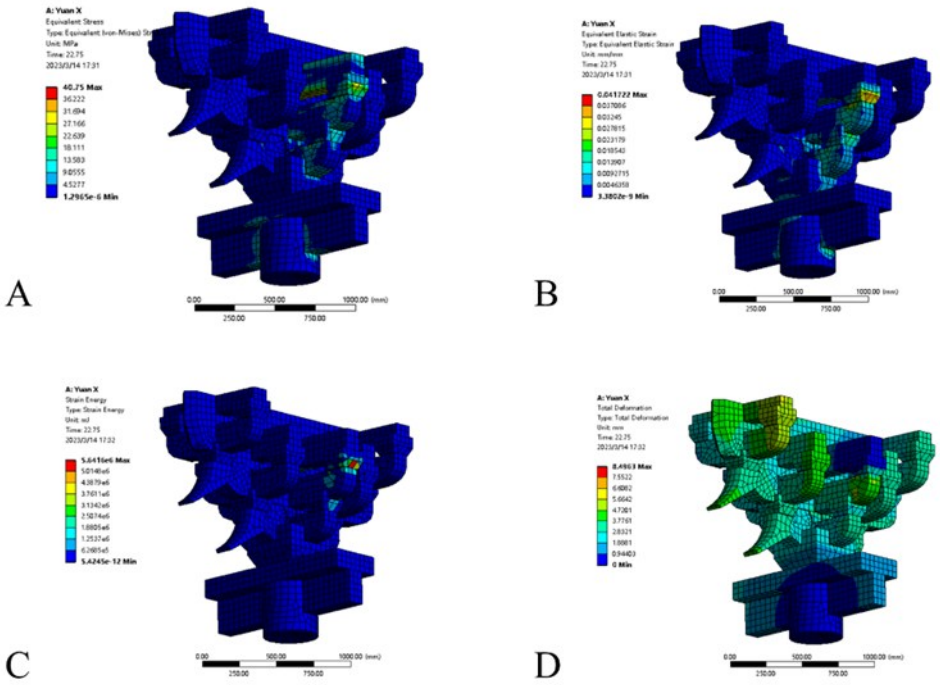

Fig. 12. Von Mises equivalent stress, equivalent elastic strain, strain energy, and Y-axis global deformation contour plots

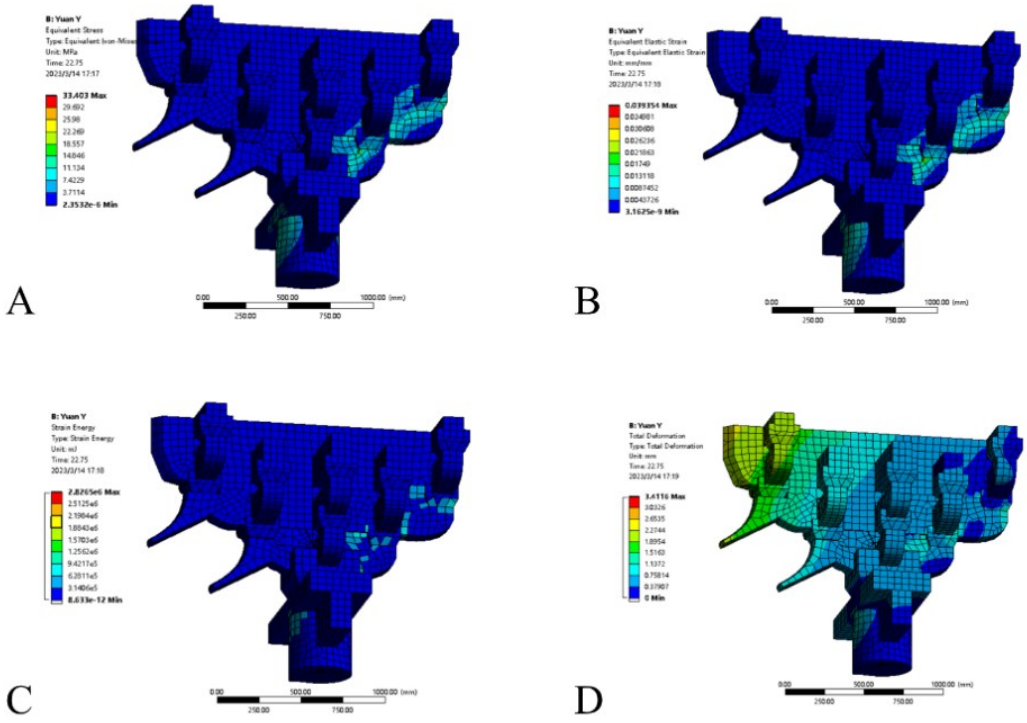

Fig. 13. X-axis Von Mises equivalent stress, equivalent elastic strain, strain energy and global deformation contour plots

The stress distribution according to von Mises is illustrated in Fig. 12A, which reveals pronounced stress concentration. This stress concentration is primarily confined to the interface between Huagong/beam and Sandou connection. The maximum stress value recorded was 33.4 MPa, which was specifically observed at the junction between the rear of Huagong and Sandou. The distribution of equivalent elastic strain is similar to that of the stress contour plot (Fig. 12B), with a maximum strain value of 0.0393 concentrated at the junction between the rear of the Huagong and the Sandou. The distribution of strain energy density (Fig. 12C) aligns with that of the stress contour map, confirming the effective transfer of energy from the upper structure through the dougong system to the supporting columns. The highest energy was recorded at the junction between the rear of the Huagong and the Sandou, with a maximum cumulative strain energy of 2.83×10^6 MJ. Consequently, displacement analysis (Fig. 12D) confirms that this region is a key area for energy dissipation, exhibiting a distinct hierarchical deformation sequence: the greatest displacement occurs at the junction between the rear section of Huagong and Sandou, with a maximum displacement value of 3.41 mm. Secondary deformation gradients are concentrated at the interfaces between Liaoyanfang, Linggong, Sandou, Ludou and column-head interfaces.

The equivalent stress distribution under quasi-static loading from horizontal low-cycle cyclic loading along the x-axis in the simulation model (Fig. 13A) reveals critical stress concentrations at the junctions between the *Nidaogong*, *Mangong*, and the *Luohanfang* with the *Sandou*. The maximum stress concentration occurs at the mortise-and-tenon joint between the right *Nidaogong* and the *Sandou*, with peak stress values reaching 40.8 MPa. This stress distribution bears a resemblance to the equivalent elastic strain distribution (Fig. 13B), reaching its maximum value at the mortise-and-tenon joint where the right *Nidaogong* meets the *Sandou* junction, with a peak value of 0.0417. The strain energy (Fig. 13C) similarly follows the stress distribution pattern, reaching its maximum value of 5.64×10^6 MJ at the junction between the right *Mangong* and the *Sandou*. This phenomenon of energy concentration indicates that the predominant energy dissipation during load cycling occurs at the joints of the mortise-and-tenon components. The model depicting the overall deformation displacement of the dougong (Fig. 13D) indicates that the maximum displacement of 8.50 mm occurs at the mortise-and-tenon joint between the right *Mangong* and the *Sandou*. The overall deformation is predominantly distributed in the upper section of the entire structure, with the deformation gradually diminishing towards the foundation. The observed results bear a marked resemblance to the known deformation patterns under lateral loading in traditional timber structures. It is noteworthy that the stress-strain-energy simulation model indicates that the greatest deformation may occur at the mortise-and-tenon joint where the *Nidaogong* meets the *Sandou*, potentially leading to its failure. stress and strain energy at this joint node exceeded the safety limits for comparable timber connections, its failure mode aligns with the failure patterns historically documented in traditional timber structures subjected to cyclic lateral loading.

Static Behavior Model of Yuan Dynasty Dougong on the Z-, Y-, and X-Axes

The Dougong of the fifth-storey exterior eaves columns-head of the Yanghe Tower during the Yuan Dynasty exhibited a three-stage degradation of elastic stiffness under monotonic loading along the Z-axis (Fig. 14), demonstrating three distinct mechanical characteristics. During the OA stage (0–ΔA), the original minute gaps between the Dougong components closed, resulting in non-linear contact. However, the structural

stiffness generated was low (K_{OA} = 1.47 kN/mm, calculated *via* Eq. 1). During the AB stage (ΔA-ΔB), elasticity develops linearly, at which point the Dougong system exhibits stable stiffness (K_{AB} = 2.25 kN/mm, derived from Eq. 2). During the BC stage, interactions between components cause elastic stiffness to transform into plastic stiffness (K_{BC} = 2.08 kN/mm, per Eq. 3) forming the BC stage (ΔB–ΔC). This arises from the yielding of mortise-and-tenon joints and the cumulative damage leading to component destruction.

$$k_{OA} = \frac{P_x}{\Delta_x} \quad (1)$$

$$k_{AB} = \frac{P_y - P_x}{\Delta_y - \Delta_x} \quad (2)$$

$$k_{BC} = \frac{P_b - P_y}{\Delta_b - \Delta_y} \quad (3)$$

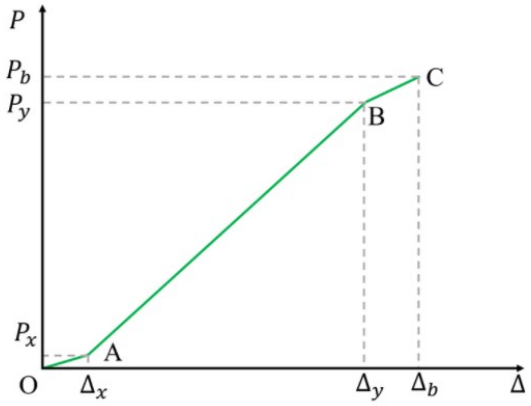

Fig. 14. Linear elastic mechanical model of Yuan Dynasty dougong under monotonic vertical static loading along the Z-axis

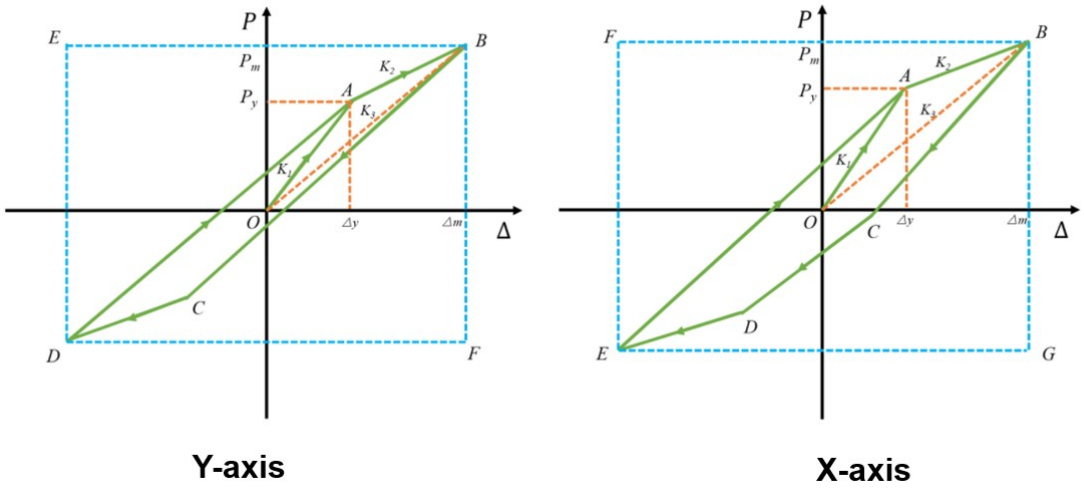

Fig. 15. Static behaviour model of Yuan Dynasty Dougong on the y-axis and x-axis

Based on the stiffness degradation curves and skeletal curves of the dougong along the Y-axis and X-axis, a static behaviour model was established for the fifth-storey eave column head dougong experimental model of the Yanghe Tower from the Yuan Dynasty along both the Y-axis and X-axis (Fig. 15).

On the Y-axis, the segment OA represents the elastic deformation stage, where the load applied to the test model is directly proportional to displacement. The elastic stiffness K_{Y1} established on the Y-axis is 10.0 kN/mm; Stages AB represent the transition of the component from elastic to plastic deformation (yield stage). From point A to point B, the component undergoes reversible plastic deformation under applied force. The test model's stiffness measures 6.41 kN/mm (KY2) at this phase, while its effective stiffness (KY3)—the ratio of the recovery model's peak load to its maximum displacement—reaches 12.0 kN/mm. The static behavior model of the Yuan Dynasty dougong experimental model along the X-axis is analogous to that along the Y-axis. The elastic stiffness K_{X1} during the elastic stage OA is 13.5 kN/mm; the plastic stiffness K_{X2} during the yield stage AB is 2.67 kN/mm, with an effective stiffness K_{X3} of 7.57 kN/mm.

The dougong brackets serve both load-bearing and seismic load-transferring functions. Consequently, they may be regarded as damping devices within ancient Chinese timber structures, supporting the roof while transferring loads to the columns. To quantitatively assess their damping performance, the nonlinear coefficient (NL) is calculated as the ratio of the area enclosed by the hysteresis curve in Fig. 15 to the area of rectangle S_{BDEF}. This coefficient characterises the energy dissipation behaviour of dougong components. The nonlinear coefficient NL on the Y-axis and the nonlinear coefficient NL on the X-axis for the experimental restoring force model of the fifth-store external eaves Dougong bracket components were 0.131 and 0.236 respectively.

The ductility of the Dougong member is characterized by the ratio between its ultimate displacement and yield displacement, which serves as an index for deformation capacity. A higher ductility value indicates superior deformation capacity of the component. Based on the test results from the simulation model, the ductility of the five-layer external eave Dougong bracket assembly test specimen was 2.59 in the Y-axis direction and 3.59 in the X-axis direction.

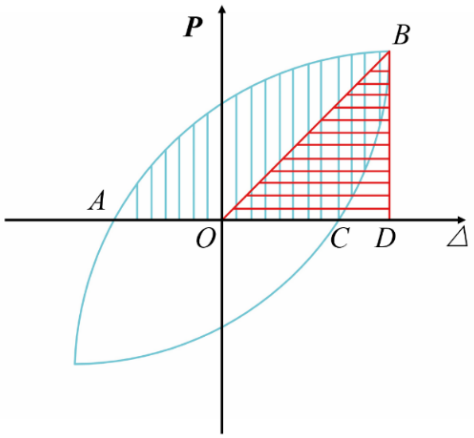

Fig. 16. Calculation of equivalent viscous damping coefficient

The higher the value of the equivalent viscous damping coefficient (h_e), the greater the energy dissipation capacity of the Dougong bracket component. The equivalent viscosity damping coefficient is calculated according to Fig. 16 and Eq. 4. In the equation,

h_e denotes the equivalent viscous damping coefficient, while S_{abc} and S_{obd} represent the areas of the corresponding shapes respectively. For the five-layer external cornice column-head Dougong bracket test model, the equivalent viscosity damping coefficients in the Y-axis and X-axis directions are 0.072 and 0.144 respectively.

$$h_e = \frac{1}{2\pi} \cdot \frac{S_{ABC}}{S_{OBD}} \quad (4)$$

Employing three-dimensional modelling techniques, the static structural performance and stress-strain distribution of the Dougong bracket at the fifth-store exterior eaves columns-head of the Yanghe tower from the Yuan dynasty were analyzed along its three principal axes (X, Y, Z). Under the action of a vertically monotonic static load applied along the Z-axis, the behavior exhibited by the structure conforms to a line-elastic model with variable stiffness. The resulting mechanical characteristics are divided into three stages: Stage I involves the compaction treatment of gaps between components and node connections; The stage II structure is in a linear phase, where load-displacement develops linearly and stiffness remains constant; and stage III of the dougong structure yielded until it failed. Along the Y-axis and X-axis directions, the structural behavior under horizontal low-cycle cyclic loading conforms to a multilinear restoring force model, exhibiting a progressive sequence of elastic, yield, and failure stages. During loading, a gradual reduction in stiffness within the support system was revealed. Near the coordinate origin, the hysteresis loop exhibited compression, demonstrating characteristics of slip. Once the horizontal load exceeds the critical value, it will induce severe plastic deformation accompanied by a rapid increase in displacement. The triaxial evaluation quantifies the component's key mechanical properties in terms of strength, deformation, and energy dissipation, with key parameters as shown in Table 2. The experimental results indicate that when subjected to excessive loads, critical structural nodes commence failure, whereupon forces are redistributed, leading to the progressive collapse of the Dougong bracket system.

Table 2. Key Mechanical Parameters of Yuan Dynasty Dougong Brackets

Name	Yanghe Tower in Yuan Dynasty					
Pathway	Simulation, structural testing					
Intensity		Deformation			Energy dissipation	
F_{Z1}	F_{Z2}	K_{Z1}	K_{Z2}	K_{Z3}	NL(Y)	
306.78	342.91	1.47	2.25	2.08	0.131	
F_{Y1}	F_{Y2}	K_{Y1}	K_{Y2}	K_{Y3}	NL(X)	
736.85	736.85	10.05	6.41	12.03	0.236	
F_{X1}	F_{X2}	K_{X1}	K_{X2}	K_{X3}	H_Y	
523.47	523.47	13.47	2.67	7.57	0.072	
		U_Y	U_X		H_X	
		2.59	3.59		0.144	

* F_{Z1} and F_{Z2} denote the yield and ultimate bearing capacities (in kN), respectively, under Z-axis loading. Similarly, F_{Y1} and F_{Y2} indicate the maximum positive and negative horizontal thrusts (in kN) along the Y-axis, while F_{X1} and F_{X2} represent those along the X-axis. In terms of stiffness parameters under Z-axis loading, K_{Z1} corresponds to the initial stiffness, K_{Z2} to the yield stiffness, and K_{Z3} to the ultimate stiffness (all in kN/mm). For Y-axis loading, K_{Y1}, K_{Y2}, and K_{Y3} refer to the elastic, plastic, and effective stiffnesses (in kN/mm), respectively. Likewise, K_{X1}, K_{X2}, and K_{X3} describe the elastic, plastic, and effective stiffnesses (in kN/mm) under X-axis loading. The ductility values along the Y and X axes are represented by U_Y and U_X, respectively. Nonlinear coefficients in the Y- and X-axis directions are designated as NL(Y) and NL(X), while H_Y and H_X correspond to the equivalent viscous damping coefficients along the respective axes.

CONCLUSIONS

1. The experimental model of the 'five-tiered outer eave column head Dougong bracket' from the Yanghe Tower (Yuan Dynasty) exhibits static structural behaviour consistent with the variable stiffness linear elastic model under vertical monotonic static loading along the Z-axis. Consequently, this behaviour may be described using the variable stiffness linear elastic model. The static structural behaviour under quasi-static loading from low-cycle reciprocating loads along the Y-axis is analogous to that under quasi-static loading from low-cycle reciprocating loads along the X-axis. Both conform to the restoring force model and may thus be described by this approach.
2. In terms of strength levels, the Yuan Dynasty bracket test model exhibited a yield bearing capacity of 307 kN under Z-axis loading and an ultimate bearing capacity of 343 kN under Z-axis loading; The maximum horizontal thrust in both positive and negative directions when loaded along the Y-axis was identical at 737 kN; The maximum horizontal thrust in both positive and negative directions when loaded along the X-axis was identical at 523 kN.
3. At the deformation level, the initial stiffness of the Z-axis loading member in the Yuan Dynasty bracket test model was 1.47 kN/mm, its yield stiffness was 2.25 kN/mm, and its deformation stiffness was 2.08 kN/mm. For the Y-axis loading member of the Yuan Dynasty bracket test model, the elastic stiffness was 10.0 kN/mm, the plastic stiffness was 6.41 kN/mm, the effective stiffness was 12.0 kN/mm, and the ductility along the Y-axis was 2.56. The elastic stiffness of the loaded member in the X-axis direction of the Yuan Dynasty bracket test model is 13.5 kN/mm. The plastic stiffness of the loaded member in the X-axis direction is 2.67 kN/mm. The effective stiffness of the loaded member in the X-axis direction is 7.57 kN/mm. The ductility of the member in the Y-axis direction is 3.59.
4. In terms of energy dissipation, A value of 0.131 was obtained for the nonlinear coefficient along the Y-axis in the Yuan Dynasty dougong bracket test model, with an equivalent viscous damping coefficient of 0.072 along the Y-axis. Along the X-axis, the nonlinear coefficient is 0.236, with an equivalent viscous damping coefficient of 0.144.
5. Through finite element analysis, comprehensive mechanical properties were determined: ultimate load-bearing capacity of 343 kN and ductility of 3.59. This successfully demonstrated the structural functionality of the Dougong bracket-support system, verifying that the Yuan dynasty architects' Dougong bracket design constituted a mechanically optimised solution. It achieved a balanced coordination between the efficiency of transmitting roof loads through the brackets and seismic resistance.

ACKNOWLEDGMENTS

This work was supported by the National Natural Science Foundation of China-Regional Science Foundation Project 'Construction of Static Structural Performance Evaluation System for *Five-tier Outer Eave Column-head Dougong Bracket* Components (32360356), the Scientific Research Projects of First-class Disciplines (Grant No. YLXKZX-NKD-027), and the Fundamental Research Funds for Inner Mongolia University of Science & Technology (Grant No. 2024QNJS023).

Use of Generative AI

This article employed the artificial intelligence tool Deepseek to refine the text.

REFERENCES CITED

Bedon, C., Rinaldin, G., and Fragiacomo, M. (2015). "Non-linear modelling of the in-plane seismic behaviour of timber Blockhaus log-walls," *Engineering Structures* 91, 112-124. https://doi.org/10.1016/j.engstruct.2015.03.002

Cao, J., Li, X., Liu, Y., Qian, H., and Yu, D. (2022). "Seismic performance investigation of the Dou-gong joints of traditional Chinese timber structures," *European Journal of Wood and Wood Products* 81(1), 173-186. https://doi.org/10.1007/S00107-022-01863-X

Chen, C., Li, Y., Han, D., Kang, H., and Li, Y. (2025). "Simulation study on the static characteristics of 'Five-tier Outer Eave Column-head Dougong Bracket' from the main hall of Nanchan Temple in Tang Dynasty," *BioResources* 20(3), 6082-6099. https://doi.org/10.15376/biores.20.3.6082-6099

Chen, J., Chen, Y., Shi, X., Zhao, Y., and Li, T. (2018). "Hysteresis behavior of traditional timber structures by full-scale tests," *Advances in Structural Engineering* 21(2), 287-299. https://doi.org/10.1177/1369433217717117

Christovasilis, I. P., Filiatrault, A., Constantinou, M. C., and Wanitkorkul, A. (2009). "Incremental dynamic analysis of woodframe buildings," *Earthquake Engineering & Structural Dynamics* 38(4), 477-4, 96. https://doi.org/10.1002/eqe.864

Deng, Y., Li, Y., and Li, Ai. (2023). "Seismic safety assessments of historical timber buildings using updated finite element models: Case study of Yingxian wooden pagoda, China," *Journal of Building Engineering* 63(PA). https://doi.org/10.1016/j.jobe.2022.105454

GB/T 15777 (2017). "Method for determination of the modulus of elasticity in compression parallel to grain of wood," Standardization Administration of China, Beijing, China.

GB/T 1933 (2009). "Method for determination of the density of wood," Standardization Administration of China, Beijing, China.

GB/T 1935 (2009). "Method of testing in compressive strength parallel to grain of wood," Standardization Administration of China, Beijing, China.

GB/T 1936.1 (2009). "Method of testing in bending strength of wood," Standardization Administration of China, Beijing, China.

GB/T 1939 (2009). "Method of testing in compression perpendicular to grain of wood," Standardization Administration of China, Beijing, China.

GB/T 1943 (2009). "Method for determination of the modulus of elasticity in compression perpendicular to grain of wood," Standardization Administration of China, Beijing, China.

Kaori, F. (2019). "Dynamic performance of bracket complexes used in traditional timber structures in Japan," *Proceedings of the Japan Academy. Series B, Physical and Biological Sciences* 95(9), 568-580. https://doi.org/10.2183/pjab.95.038

LY/T 3297 (2022). "Dynamic test method for shear modulus of wood," Standardization Administration of China, Beijing, China.

Meng, X., Li, T., and Yang, Q. (2019). "Experimental study on the seismic mechanism of a full-scale traditional Chinese timber structure," *Engineering Structures* 180, 484-

493. https://doi.org/10.1016/j.engstruct.2018.11.055

Meng, X., Yang, Q., and Wei, J. (2018). "Experimental investigation on the lateral structural performance of a traditional Chinese pre-Ming dynasty timber structure based on half-scale pseudo-static tests," *Engineering Structures* 167, 582-591. https://doi.org/10.1016/j.engstruct.2018.04.077

Niu, Q. (2017). *Experimental Study and Theoretical Analysis on Half-Scale Model of Timber Structure in Song Dynasty*, Master's Thesis, Taiyuan University of Technology, Taiyuan, China.

Ou, T., and Wang, D. (2023). "Study on seismic performance of base-isolated and base-fixed Ancient timber buildings in hanging-wall/footwall earthquakes," *Journal of Asian Architecture and Building Engineering* 22(2), 374-389. https://doi.org/10.1080/13467581.2022.2045999

Sha, B., Xie, L., Yong, X., and Li, A. (2021). "Hysteretic behavior of an ancient Chinese multi-layer timber substructure: A full-scale experimental test and analytical mode," *Journal of Building Engineering* 43. https://doi.org/10.1016/j.jobe.2021.103163

Song, X., Wu, Y., Li, K., Jin, L., Chen, F., Liu, X., and Dou, X. (2019). "Mechanical behavior of a Chinese traditional timber pagoda during construction," *Engineering Structures* 196, article 109302. https://doi.org/10.1016/j.engstruct.2019.109302

Wu, C., Xue, J., Song, D., and Zhang, Y. (2022). "Seismic performance evaluation of a roof structure of a historic Chinese timber frame building," *International Journal of Architectural Heritage* 16(10), 1474-1495. https://doi.org/10.1080/15583058.2021.1894503

Xian, R., Zhao, B., Wu, Y., Xie, Q., Liu, Y., and Wang, X. (2025). "Seismic performance of traditional Chinese timber structure: A case of Guangyue tower," *Journal of Building Engineering* 100, article 111690. https://doi.org/10.1016/j.jobe.2024.111690

Xue, J., Liang, X., Wu, C., Song, D., and Qi, L. (2022). "Experimental and numerical study on eccentric compression performance of Dou-Gong brackets at column tops," *Structures* 35, 608-621. https://doi.org/10.1016/j.istruc.2021.11.035

Yao, L. and Li, Y. (2023). "Simulation study on static characteristics of Qing-style 'One Bucket Three Liters' column-cap Dou-Gong bracket," *BioResources* 18(4), 6955-6970. https://doi.org/10.15376/biores.18.4.6955-6970

Zhang, B., Xie, Q., Li, S., Zhang, L., and Xue, J. (2023). "Numerical analysis of traditional Chinese timber structure: Simplified finite element model and composite elements of joints," *Journal of Building Engineering* 67. https://doi.org/10.1016/j.jobe.2023.106027

Zhang, X., Cui, L., Qi, H., Wang, H., and Lin, L. (2024). "Seismic fragility analysis of traditional Chinese timber structures based on a simplified lumped mass model considering joint damage," *Structures* 70, article 107863. https://doi.org/10.1016/j.istruc.2024.107863

Article submitted: October 13, 2025; Peer review completed: January 17, 2026; Revised version received and accepted: February 4, 2026; Published: February 19, 2026.
DOI: 10.15376/biores.21.2.3284-3299